Available online at www.sciencedirect.com
SCIENCE DIRECT®
Journal of the European Ceramic Society 25 (2005) 1663–1673
www.elsevier.com/locate/jeurceramsoc

Processing of textured zinc oxide varistors via templated grain growth

Ender Suvaci*, İ. Özgür Özer

Department of Materials Science and Engineering, Anadolu University, Iki Eylul Campus, Eskisehir, 26480 Turkey

Received 26 February 2004; received in revised form 17 May 2004; accepted 23 May 2004
Available online 13 August 2004

Abstract

Textured, dense zinc oxide varistors were successfully fabricated by Templated Grain Growth (TGG) technique. Rod-like, anisotropic ZnO particles (templates) were synthesized by homogeneous precipitation method. The templates are aligned in such a position where *c*-axes of the templates are parallel to the tape casting direction during the modified tape casting process. Since zinc oxide varistors are liquid phase sintered, addition of the templates to initial powder mixture does not result in constrained densification. The aligned zinc oxide templates grow anisotropically during sintering. $(1\,1\,\bar{2}\,0)$ and $(1\,0\,\bar{1}\,0)$ prismatic planes of the ZnO crystals (templates) grow faster than the other ZnO crystal planes. The growth of the templates results in texture development in zinc oxide varistors. As sintering temperature increases, fraction of textured grains in the microstructure increases. A template growth mechanism is also proposed for texturing zinc oxide varistors by TGG.

Keywords: ZnO; Varistors; Grain growth; Microstructure-final; Texturing

1. Introduction

Zinc oxide varistors are electroceramic devices, which are produced by sintering of zinc oxide with small amounts of metal oxides such as Bi_2O_3, Sb_2O_3, CoO, Cr_2O_3, MnO and/or TiO_2.[1–3] These devices exhibit highly nonlinear current–voltage (*I–V*) characteristics and hence they are utilized as electrical and electronic circuit protectors against power and voltage surges.[2,3] Electrical resistance of varistors decreases drastically when voltage is increased over a critical threshold voltage. When they are connected in parallel with the equipment to be protected, they divert the transients and avoid any further over voltage on the equipment. The threshold voltage, V_{th}, of the varistor is determined by $V_{th} = (N_g - 1)\,V_{gb}$ where N_g is the number of ZnO grains in series within a sample and subsequently, $N_g - 1$ is the number of grain boundaries between the electrodes, and V_{gb} is the threshold voltage of a grain boundary. This grain boundary threshold voltage is determined by composition and defect structure of the grain boundary phase and usually estimated as 2–4 V. Since the threshold voltage dictates application area (i.e., voltage rating) of the varistor, varistors for various applications can be prepared by controlling final ZnO grain size and the threshold voltage of each grain boundary. For example, Eda et al. produced low-voltage ZnO varistors with a threshold voltage of 6 V/mm. In that study, large ZnO grains (∼500 μm) were achieved by controlling grain growth via seed grains.[4] Hennings et al. also utilized seed grains to achieve a more uniform and controlled microstructure in low-voltage varistor systems.[5] In addition, Sb_2O_3 is usually utilized to inhibit grain growth in high voltage varistor ceramics;[6] however, it has been recently reported that under some conditions where Sb_2O_3 content is less than ∼30 ppm, exaggerated grain growth can also be observed even in antimony oxide-doped ZnO ceramics.[7]

The varistors exhibit three important regions in the *I–V* curve: low current linear region, intermediate current nonlinear region and high current upturn region.[3] In the first region, an ohmic (linear) *I–V* characteristic is observed and the resistance of the ZnO grain boundaries determines the *I–V* characteristics. The second intermediate current nonlinear region is the heart of the current–voltage (*I–V*) characteristic of

* Corresponding author.
E-mail addresses: esuvaci@anadolu.edu.tr, esuvaci@yahoo.com (E. Suvaci).

0955-2219/$ – see front matter © 2004 Elsevier Ltd. All rights reserved.
doi:10.1016/j.jeurceramsoc.2004.05.026

ZnO varistors, wherein the device conducts an increasingly large amount of current for a small increase in voltage. The degree of nonlinearity (represented by nonlinear coefficient, α) is determined by the flatness of the nonlinear region, the flatter the *I–V* curve (i.e., the greater α) in this region, the better the device. Although the controlling parameters for this region only qualitatively understood, *I–V* characteristics are controlled indirectly by the difference between electrical resistivity of the grain boundary and the ZnO grain.[3] The high current upturn region shows the limiting condition for protection from high current surges. Accordingly, for applications involving high magnitudes of current, varistors with high upturn current values are desirable. This region is controlled by the resistance of the ZnO grains. Therefore, dopants such as Al and Ga are utilized to enhance electrical conductivity of the ZnO grains and to shift the upturn point to higher current values.[8,9] This shift usually results in extension of nonlinear region and increase in α. Consequently, the electrical properties of ZnO varistors are directly related to their microstructure and electrical resistivities of ZnO grains and grain boundaries.

Single crystal of zinc oxide has a wurtzite type hexagonal structure. In addition, while bond type between Zn and O atoms exhibits covalent characteristic in the *c*-direction, it is mostly ionic in the *a*-direction.[10] Therefore, ZnO single crystals exhibit highly anisotropic properties. For example, the electrical resistivity of the single crystal is 3 Ω cm through *a*-axes whereas it is ∼8.2 Ω cm through *c*-axes at room temperature.[11] In thin film applications, this anisotropy has been successfully utilized in the form of textured ZnO films to enhance performance of the devices.[12,13] However, although bulk ZnO ceramics such as varistors could benefit from texturing as stated by Eda et al.[4] in 1983, there are only a few studies on texture development in bulk zinc oxide ceramics.[14,15] In one of those studies, Tani and his coworkers showed the improvement of thermoelectric performance of yttrium-substituted $(ZnO)_5In_2O_3$ electroceramics by texture development.[14]

Textured microstructures allow access to ceramics with anisotropic properties, which are similar to single crystal values.[16] Alternatively, characteristics of one orientation can be used to benefit such as in the case of α-Al_2O_3 where the faces parallel to the optical axis are harder than those perpendicular to it.[17] Earlier attempts to obtain textured ceramics involved orienting whisker, fiber or platelet-shaped particles.[18–21] Such systems had low densities and required hot pressing and sinter forging to obtain dense, textured ceramics. Recently, a process referred to as Templated Grain Growth (TGG) has been developed to circumvent the densification problem and to produce textured microstructures.[22–24] TGG can be defined as a technique for developing crystallographic texture in ceramic bodies via the grain growth of aligned anisometric (i.e., template) particles in a dense and fine grain size matrix. Initial studies of TGG concluded that thermodynamically stable template particles, the alignment of the template particles (or seeds) during forming, a fine-grain size, and a dense matrix are critical requirements for TGG.[23–25] Templates can be oriented by a variety of techniques, including tape casting, slip casting, centrifugal casting, and extrusion. After densification (i.e., >∼91% TD), these larger anisotropic grains grow to consume the matrix grains to yield ceramics with high degrees of crystallographic orientation and textured grains.[16] In addition, template loading determines the inter-template spacing and subsequently, the degree of template growth. The spacing distance can be predicted from the initial template concentration and template dimensions. That is, final grain size can be controlled readily by controlling these parameters in TGG process.

In the last few years, a variety of ceramic systems have been produced by TGG and related routes to yield textured ceramics with interesting properties.[26–29] For example oriented Si_3N_4 ceramics have been shown to yield interesting fracture characteristics and thermal conductivity.[26–28] A variety of ferroelectric ceramics (e.g., $(PbMg_{1/3}Nb_{2/3})O_3$–$PbTiO_3$, $Sr_2Nb_2O_7$, $Bi_4Ti_3O_{12}$, $Sr_{0.53}Ba_{0.47}Nb_2O_6$) have been textured by TGG.[30–33] In PMN–PT, $Bi_4Ti_3O_{12}$ and $Sr_{0.53}Ba_{0.47}Nb_2O_6$, it was shown that piezoelectric properties similar to those of single crystals can be obtained. In addition, highly textured alumina and mullite have also been produced.[22,34] Those studies showed that TGG is a versatile technique to produce textured ceramics with controlled grain size.

If polycrystalline ZnO ceramics are textured, they exhibit single crystal-like anisotropic properties which may result in superior properties in certain crystallographic directions. Since the TGG approach has been successfully utilized to induce texture and to control final grain size in various ceramic systems earlier, it can be applied for ZnO varistors. Consequently, the research objective of this study was to investigate processing of textured zinc oxide varistors by TGG process.

2. Experimental procedure

2.1. ZnO powder synthesis via homogeneous precipitation

ZnO templates, used in this study, were synthesized via homogeneous precipitation method as reported by Sakka et al.[35] Aqueous solutions of 0.01 M zinc nitrate hexahydrate ($Zn(NO_3)_2{\cdot}6H_2O$) and hexamethylene tetramine (HMT) were employed for the synthesis. $Zn(NO_3)_2{\cdot}6H_2O$ was dissolved in the distilled water and pH was reduced to 2.0 by addition of 5 wt.% HNO_3 solution. The solution was heated while it was stirred at ≈600 rpm. HMT was added as the temperature of the solution reached 70 °C. A turbidity in the solution, indicating the formation of particles was observed at 90 °C by the activation of HMT. Reaction time for 1.5 h was applied after the observation of turbidity. Products were collected by centrifuge of the suspension. The centrifuge stage was repeated for five times by renewing the

distilled water to remove impurity ions. Then the particles were dried in a drying oven at 90 °C. Morphological and chemical characterization of ZnO particles were performed by scanning electron microscope and x-ray diffractometer, respectively.

2.2. Slurry preparation and tape casting

In this study, 97% ZnO, 1% Bi_2O_3, 0.5% Co_3O_4, 0.5% SnO_2, 0.5% TiO_2 and 0.5% MnO_2 (each in moles) varistor composition was used. Reagent grades of the mentioned oxides were utilized as starting materials. Template containing slurries were prepared by removing commercial ZnO powders in an equal amount to the template content from the initial composition.

In this study, four different tape casting slurries were prepared; template free and 5, 10 and 15 wt.% template containing slurries. Those slurries were called as R, 5T, 10T and 15T, respectively. Metal oxide powders in the varistor composition were ball milled in aqueous media with yttrium stabilized zirconia (YTZ) balls for 24 h. The amount of the dispersant—25 wt.% ammonium polymethacrylate solution (Darvan-C, R.T. Vanderbilt Company, Inc.)—in the slurry was 1.45 vol.%. After the milling stage, plasticizer—polyethyleneglycol (PEG 3000)—was added to the slurry in the concentration of 6 vol.% (in solid base). It was added as received powder due to its high solubility in water at room temperature. Then, the slurry was stirred for 20 min more to achieve complete dissolution of the PEG. Afterward, binder—an aqueous solution of polyvinylalcohol (PVA) in 12.5 wt.% concentration—was added to the slurry. The concentration of the binder in the slurry was 33 vol.% (in solid base). After the addition of the binder, the slurry was ball milled for 12 h more to achieve a homogeneous slurry. The suspension was sieved through 104 μm sieve to remove air bubbles. Then it was stirred by a magnetic stirrer. While it was being stirred, the templates were added to the slurry. For effective mixing of the templates into the slurry, the slurry was stirred for additional 3 h.

Tape casting was performed by using a tape caster modified with a comb blade which is formed by an array of pins apart 0.5 mm from each other. The casting process was carried out by 400 μm blade height and 40 cm/s casting speed on a glass substrate. Tapes were dried at room temperature in a closed chamber to prevent any contamination from environment. After the drying, tape thickness was ∼250 μm. The tapes were cut into pieces and laminated (10–20 layers) under 25 MPa pressure at ≈80 °C. Laminated samples were cut into 3 mm × 1.5 mm rectangular pieces. A notation used for the samples is *xTy-c/a*, where *x*, *y* and *c*/*a* refer to the template content, sintering temperature and direction of the sample with respect to the casting direction ("*c*" refers to parallel and "*a*" refers to perpendicular directions to the tape casting direction), respectively.

Laminated samples were heated at 1 °C/min to 700 °C for binder removal. After 30 min dwell time at the peak temperature, the furnace was shut down and cooled to room temperature. Samples were sintered at 900, 1000, 1100 and 1200 °C for 2 h with a heating rate of 5 °C/min.

2.3. Characterization

Density measurements of sintered samples were done by Archimedes' method. Orientation of templates in green samples and texture development in sintered samples were characterized both by x-ray diffractometer and scanning electron microscope analysis. XRD analysis were performed with Cu $K\alpha_1$ radiation between 30° and 70°.

Texture fraction of the sintered samples was determined by Lotgering factor which is a x-ray-based semi-quantitative characterization method.[36] Lotgering factor is calculated by the following equation

$$f = \frac{p - p_0}{1 - p_0} \quad (1)$$

where f is a measure of degree of orientation, p and p_0 are the ratios of between sum of the intensities of the (0 0 l) reflections and the sum of the intensities of all ($h\,k\,l$) reflections (which occur in a certain range of theta values) for the oriented and non-oriented samples, respectively. Lotgering factor, f, is measured as 0 and 1 for random and perfectly textured samples, respectively. Texture fraction of oriented samples were characterized both from *a*- and *c*-directions. Also SEM analyses of thermally etched samples were performed from c and a directions.

3. Results and discussion

3.1. Template synthesis

Fig. 1 shows the XRD pattern of the synthesized ZnO powder. All peaks shown in the pattern are ZnO peaks, indicating that the synthesis conditions, used in this study, favored formation of phase pure ZnO. For the template particles, size and shape are as important as chemical purity. Fig. 2 exhibits SEM micrograph of the synthesized ZnO particles. The particles exhibit rod-like morphology. They are elongated in the *c*-direction as predicted by changes in peak intensity ratios in the XRD pattern. They are ∼7 μm long and ∼1 μm thick (i.e., aspect ratio of the particles is ∼7). These results are in consistent with Sakka et al. who reported that size of ZnO particles, synthesized by homogeneous precipitation from a solution containing 0.01 M zinc nitrate and 0.01 M HMT, was ∼7 μm.[35] Size and shape of the template particles are extremely important for controlling initial template alignment and subsequently final grain size and texture quality.[25] Although higher the aspect ratio results in better alignment control during forming processes, presence of too large particles in the matrix of smaller ones may degrade some varistor properties.[2,3]

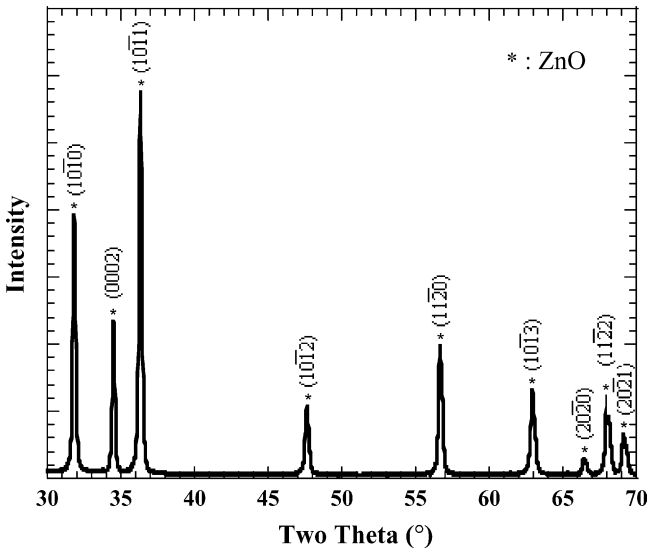

Fig. 1. XRD pattern of ZnO particles synthesized from 0.01 M zinc nitrate hexahydrate and 0.01 M HMT.

3.2. Tape casting and template alignment

Tape casting slurry was prepared by milling of commercial fine ZnO particles (∼2 μm) and other metal oxides. After 24 h milling, the average particle size of the mixture reduced to 0.6 μm. Since driving force for template growth is surface energy difference between template and matrix particles, the greater the size difference results in the greater driving force for template growth.[16,25] In addition, Suvaci and Messing showed that, in TGG-like processes, the template to matrix particle size ratio determines the thermodynamic driving force and it should be equal to at least 1.5 for template growth.[25] When the template size is compared to matrix particles after 24 h milling, the ratio becomes ∼11 in length direction and ∼1.7 in thickness direction. These results suggest that after 24 h milling of the mixture, the particle size reduction was adequate to provide thermodynamically favorable conditions for template growth. Thus, duration of the milling stage was chosen as 24 h, in this study.

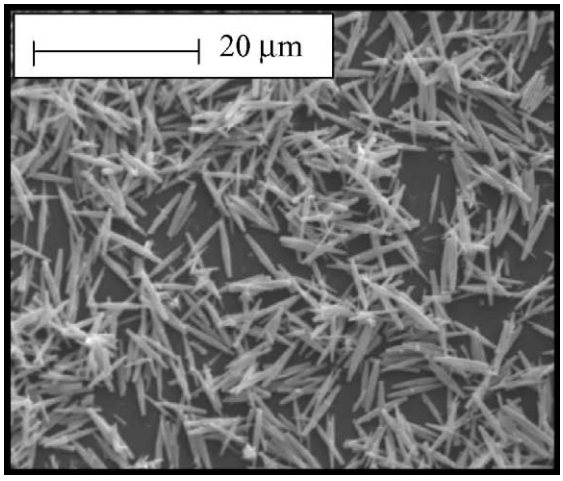

Fig. 2. SEM micrograph of ZnO particles synthesized from 0.01 M zinc nitrate hexahydrate aqueous solution.

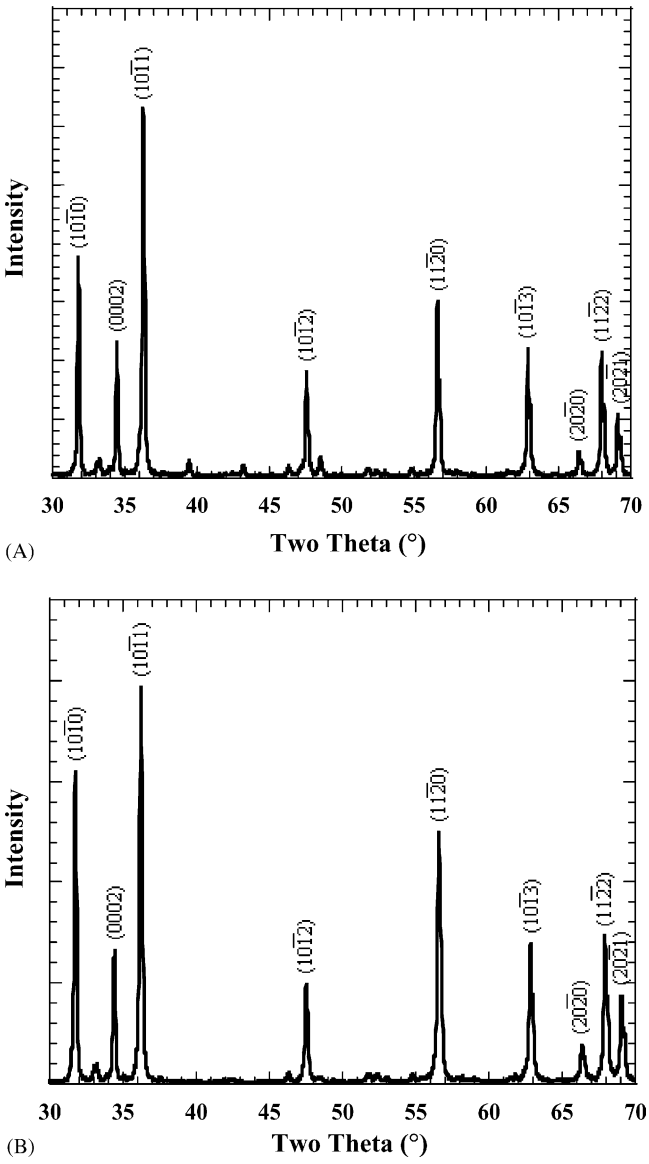

Fig. 3. XRD patterns of (A) R and (B) 10T samples before firing.

Fig. 3A and B shows the XRD patterns of the R and the 10T samples, respectively, before firing. When the patterns are closely examined, it is observed that relative intensities of the peaks are changing from one pattern to another. When intensity of the $(1\,0\,\bar{1}\,0)$ peak to intensity of the $(1\,0\,\bar{1}\,1)$ peak (i.e., the highest intensity peak for random sample) ratio is calculated for those patterns, it is found that the peak intensity ratios are 0.60 and 0.80 for the R and the 10T samples, respectively. This result implies that templates are aligned during the tape casting process. In addition, a higher relative intensity for the $(1\,1\,\bar{2}\,0)$ peak (i.e., the other prismatic plane) is observed in the XRD pattern of 10T sample. Since

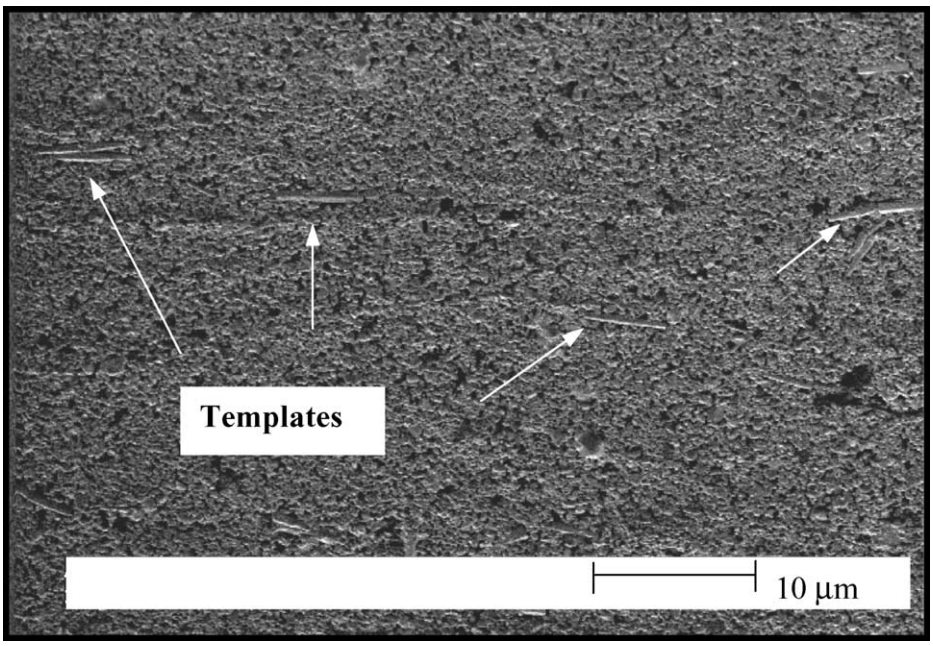

Fig. 4. SEM micrograph of 5T sample before firing.

the XRD patterns were obtained from top of the tapes and relative intensities of $(1\,0\,\bar{1}\,0)$ and $(1\,1\,\bar{2}\,0)$ peaks are higher in the template containing system than that of the template free system, it can be concluded that the prismatic planes of the templates are aligned in a direction perpendicular to the tape casting direction. Moreover, SEM micrographs demonstrate well alignment of templates parallel to the tape casting direction (i.e., *c*-axes of templates are parallel to the tape casting direction) as shown in Fig. 4 for the 5T sample. This alignment was achieved by using a modified tape casting by using an array of pins. Although effect of the pins on template alignment has not been investigated systematically in this study, significant improvement in alignment was achieved by using an array of pins. Park and Kim showed that torque for aligning whiskers was increased by n^2 times by dividing the flow into n narrow ones. Accordingly, in their samples prepared by employing the pins exhibited better whisker alignment that samples prepared by plain tape casting.[37] In addition, these results indicate that the aspect ratio of templates (i.e., ∼7) was high enough for achieving template alignment during the tape casting.

3.3. Sintering and texture development

Fig. 5 demonstrates the densification behavior of the R, 5T, 10T and 15T samples as a function of sintering temperature. After sintering at 1200 °C for 2 h the R sample exhibits 98 ± 1% TD, on the other hand other template containing systems exhibit 96 ± 1% TD. In all samples, the template particles do not appear to constrain densification, probably because stresses do not develop in the presence of the liquid.[38]

All samples exhibit relative densities >91% TD in all sintering conditions. Initial TGG studies showed that only limited template growth occurs up to ∼91% theoretical density, due to effect of grain connectivity and the presence of porosity.[25] In addition, the limited template growth below the critical density could be attributed to nonuniform wetting of anisometric particles[39] or pinning of grain boundaries by pores as suggested by Burke.[40] Burke postulated that there is a limiting density of ∼90% of theoretical for the onset of abnormal grain growth when pores are the only second phase inhibiting growth and the average pore diameter is about one-tenth the size of the grains.[40] He also reported that when

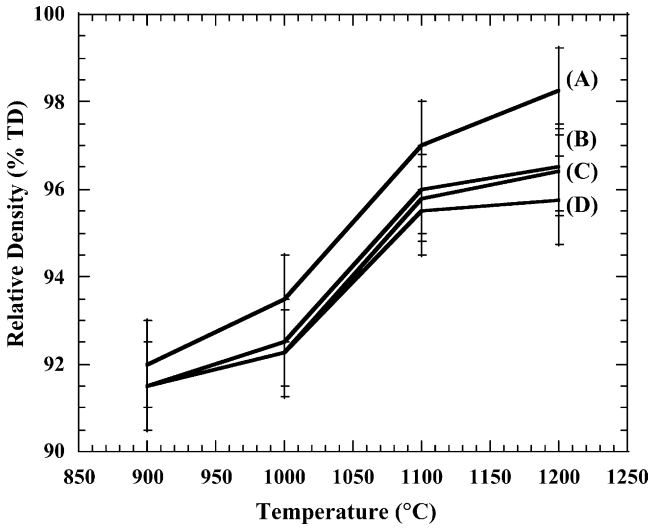

Fig. 5. Relative densities of (A) R, (B) 5T, (C) 10T, (D) 15T samples as a function of temperature.

second phases are present with pores, the onset density for abnormal grain growth is higher than ∼90%. The limiting density concept was reported for anisotropic grain growth in pure alumina.[41] Horn et al. reported that anisotropic grain growth of platelike bismuth titanate ($Bi_4Ti_3O_{12}$) was limited until the matrix density was ∼90% of theoretical.[32] Since all samples used in this study exhibited relative densities greater than ∼91% TD in all conditions, the requirement of dense matrix was satisfied with all samples. That is, the experimental conditions, chosen for this study, was favoring template growth.

Figs. 6A and B shows the microstructures of R and 10T samples, respectively, after sintering at 1200 °C for 2 h. In the microstructure of the R sample there are mostly equiaxed grains within a size range of 5–20 μm. In addition, some anisotropically grown grains are observed. Initial studies on sintering of TiO_2-doped ZnO system by Trontelj et al. showed that presence of dissolved TiO_2 in Bi_2O_3 liquid phase enhances the reactivity of the liquid phase toward the ZnO matrix. This increase in the reactivity results in increases relative velocity of prismatic planes over other planes of ZnO and hence anisotropic grain growth is observed in TiO_2 added ZnO systems.[42] In addition, Makovec et al. reported that exaggerated grain growth is triggered by the formation of Bi_2O_3-based liquid phase in reaction between $Bi_4Ti_3O_{12}$ and ZnO, and that nucleation and growth of large anisotropic grains is influenced by presence of inversion boundaries in ZnO grains.[43] Furthermore, recent reports from Daneu and coworkers also conclude that the inversion boundaries have a profound effect on the grain growth and microstructure development in ZnO-based ceramics doped with Sb_2O_3 or SnO_2.[7,44] The SEM micrograph of the 10T sample exhibits large aligned anisometric particles (i.e., 30–40 μm × 10–20 μm) as well as fine (∼5 μm) matrix grains. In this microstructure large grains are the grown template particles. It should be noted that, the template grains grow faster in prismatic plane direction than the *c*-direction and hence in the final microstructure grains appear to be aligned in *a*-direction. In addition, the preferred growth of matrix grains in this direction is observed. These results suggest that the template particles do not only induce texture but also orient matrix particles in certain growth directions and thus they regulate the final microstructure of the ZnO varistor.

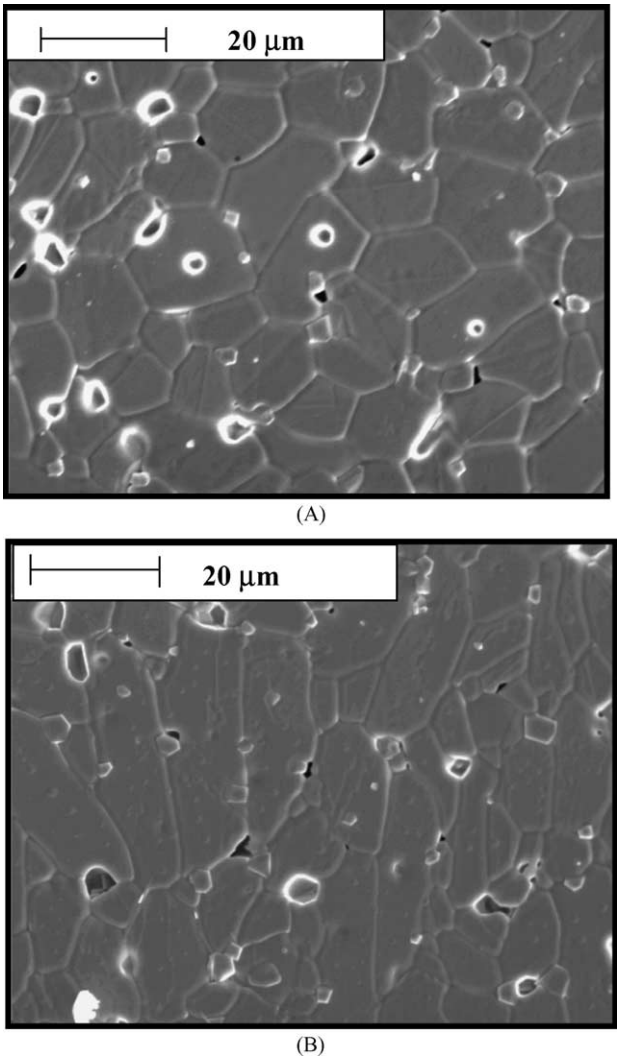

Fig. 6. SEM micrographs of (A) R and (B) 10T samples after sintering at 1200 °C for 2 h.

Figs. 7A and B shows SEM micrographs of 10T sample from *a*-direction (i.e., top view, 10T1100-a) and *c*-direction (i.e., edge view, 10T1100-c), respectively, after sintering at 1100 °C for 2 h. The XRD patterns obtained from these samples and R1100 sample are shown in Fig. 8. While Fig. 7A exhibits large, anisometric aligned grains, Fig. 7B shows mostly equiaxed grains. When the XRD patterns of R1100, 10T1100-c and 10T1100-a are closely examined, it is observed that while intensity of (0 0 0 2) peak increases, the other peak intensities decrease in the 10T1100-c sample (Fig. 8). On the other hand, in the 10T1100-a system intensities of $(1\,0\,\bar{1}\,0)$ and $(1\,1\,\bar{2}\,0)$ peaks increase whereas the other peaks diminish. These results obtained from the XRD and SEM studies confirm the development of both morphological and crystallographic texture in templated ZnO varistor ceramics. The texture achieved in this study can be called as fiber texture since the texture is controlled only in one particular direction (i.e., *c*-direction).[16]

Although high degree of texture was achieved in this study, the microstructure homogeneity still needs to be improved for varistor applications. That is, the microstructure should contain only the same-sized grains. When large grains are present in much finer matrix of varistor ceramics, they cause channels of lower resistance and broad distribution of nonlinear coefficient. In addition, current localization along such channels of lower resistance results in degradation of varistor. Therefore, it is critical to understand the effect of processing parameters on microstructure development in templated ZnO-based varistor systems to achieve a uniform and textured microstructure.

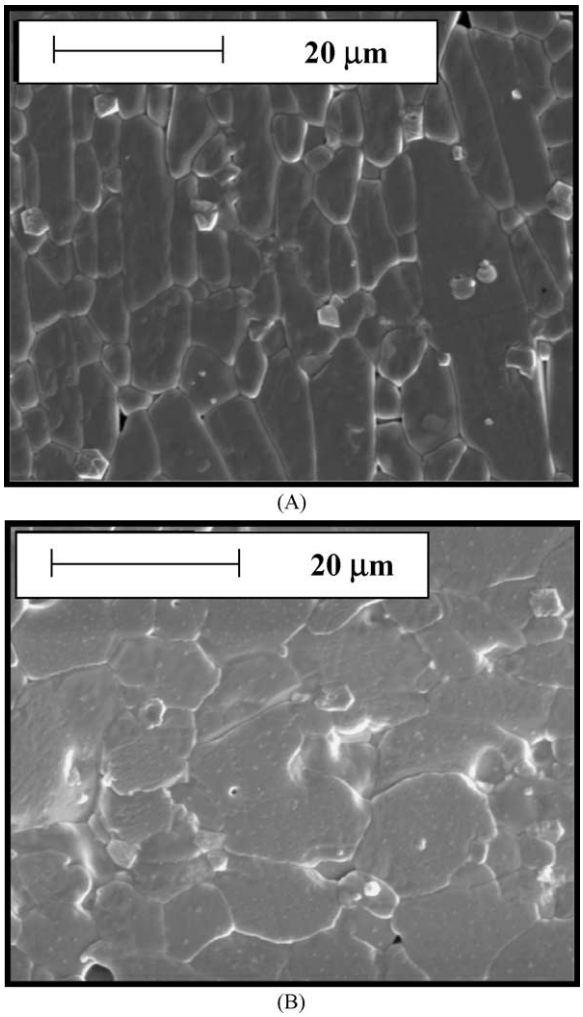

Fig. 7. (A) Top and (B) edge views of 10T sample after sintering at 1100 °C for 2 h.

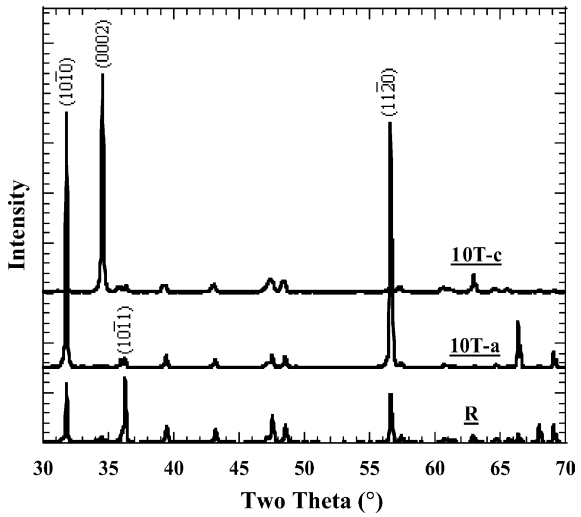

Fig. 8. XRD patterns of R, 10T-a and 10T-c samples after sintering at 1100 °C for 2 h.

3.4. Effect of sintering temperature on texture development

Texture development as a function of sintering temperature was analyzed based on the XRD patterns taken from 10T-a and 10T-c samples, after sintering at various temperatures from 900 to 1200 °C for 2 h (Fig. 9). The XRD patterns of 10T-a samples show that as the temperature increases, relative intensities of (1 0 $\bar{1}$ 0) and (1 1 $\bar{2}$ 0) peaks increase. On the other hand, in the 10T-c samples, relative intensity of (0 0 0 2) peak increases with increasing sintering temperature. These results indicate that when sintering temperature increases, degree of texture increases in those samples. Similar results were obtained for 5T and 15T samples. Lotgering factors calculated from the XRD patterns to quantify these results. For example, Lotgering factors for the 5T samples, sintered at 900, 1000, 1100 and 1200 °C were 0.55, 0.62, 0.80 and

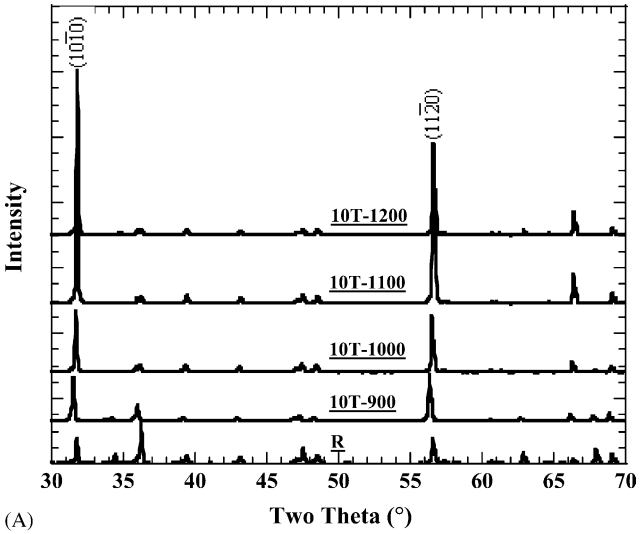

(A)

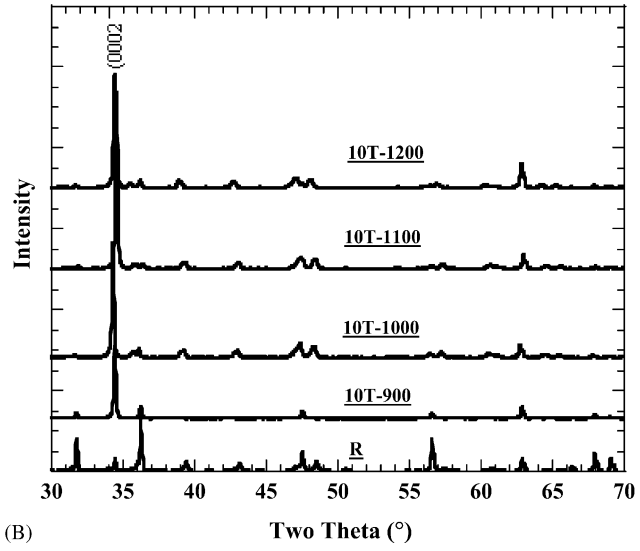

(B)

Fig. 9. XRD patterns of (A) 10T-a and (B) 10T-c samples after sintering at different temperatures for 2 h.

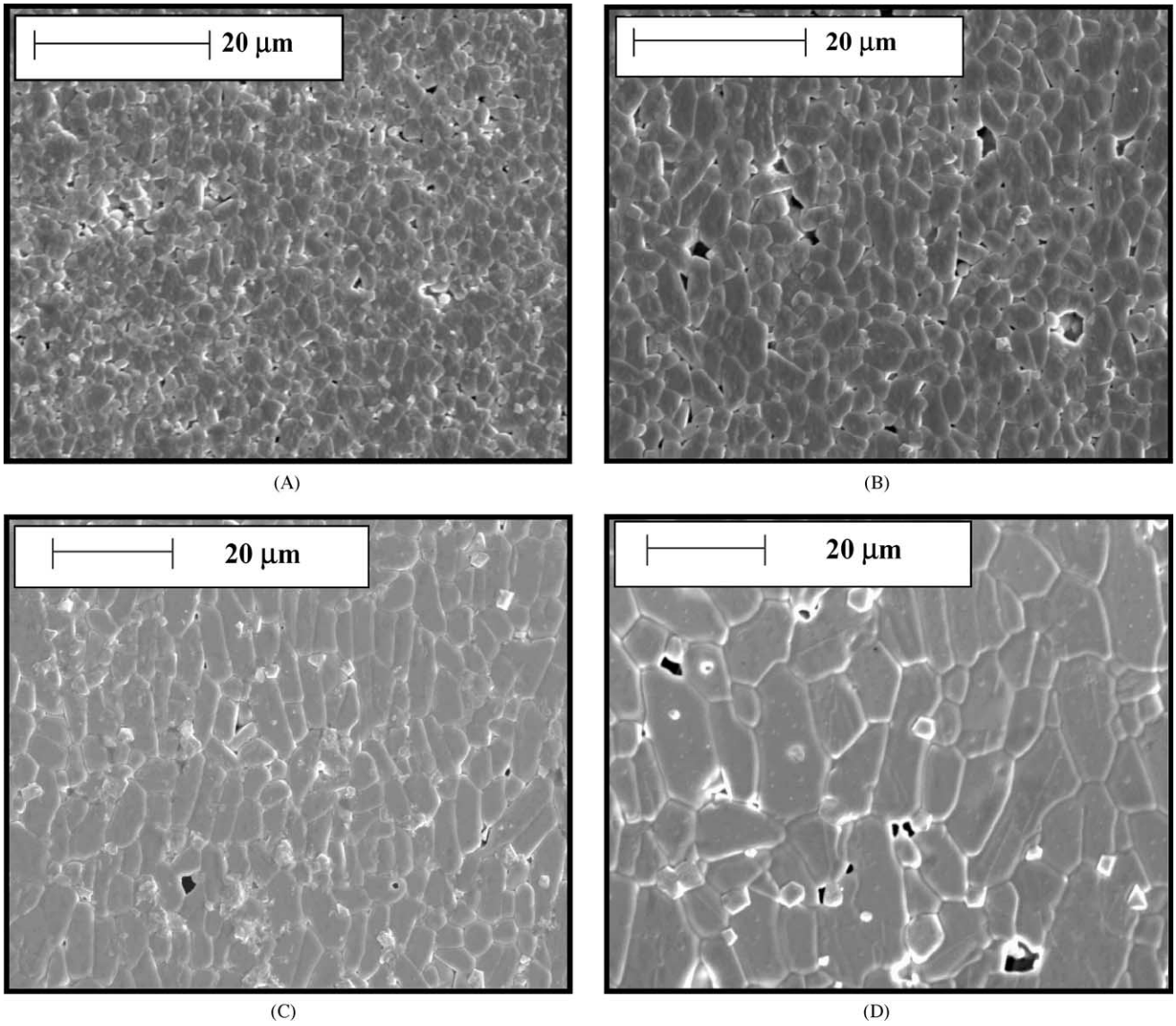

Fig. 10. SEM micrographs of 15T-a samples after sintering at (A) 900 °C, (B) 1000 °C, (C) 1100 °C and (D) 1200 °C for 2 h.

0.85, respectively. Fig. 10 shows the effect of sintering temperature on microstructure development for 15T-a samples. These SEM micrographs demonstrate that as the temperature increases, fraction of fine matrix grains decreases and large template grains grow in the expense of fine matrix grains. Therefore, fraction of textured grains in the microstructure increases with increasing sintering temperature. It should be noted that, the template particles can not be distinguished from the matrix grains readily even after sintering at 900 °C for 2 h (Fig. 10A). This suggests that even at this temperature template particles exhibit certain degree of anisotropic grain growth and their morphology switches from elongated (in *c*-direction) one to an equiaxed one. As shown in Figs. 10 C and D, further anisotropic growth of templates results in elongation of template grains in *a*-direction and hence, morphological texture development in the system.

Anisotropic template growth is observed in all samples. Although initial template size is 1 μm × 7 μm (i.e., *a*-direction dimension × *c*-direction dimension) after the sintering at 1200 °C, 2 h average size of anisotropic grains becomes ∼25 μm × 9 μm. That is, prismatic planes grow faster than basal planes. It should be noted that, above 1000 °C, the anisotropic template growth is much more pronounced. This results in a significant increase in textured fraction when the temperature changes from 1000 to 1100 °C as predicted by XRD and SEM. This change in nature of grain growth in ZnO–Bi_2O_3–TiO_2 system has also been previously reported by Makovec and coworkers.[43,45] They showed that ZnO grains are covered by a Bi and Ti rich layer above ∼760 °C. ZnO and $Bi_4Ti_3O_{12}$ react at ∼1040 °C, resulting in a Zn_2TiO_4-type spinel phase and a Bi_2O_3 liquid phase. Grain growth is retarded at $T < \sim 850$ °C, while above

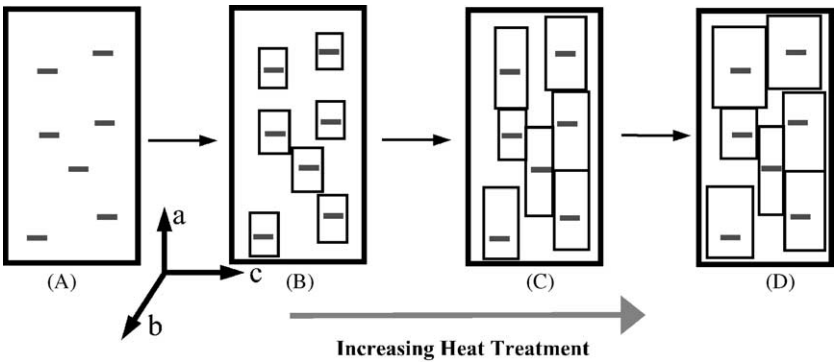

Fig. 11. Schematic illustration of anisotropic template growth in ZnO-based varistor system.

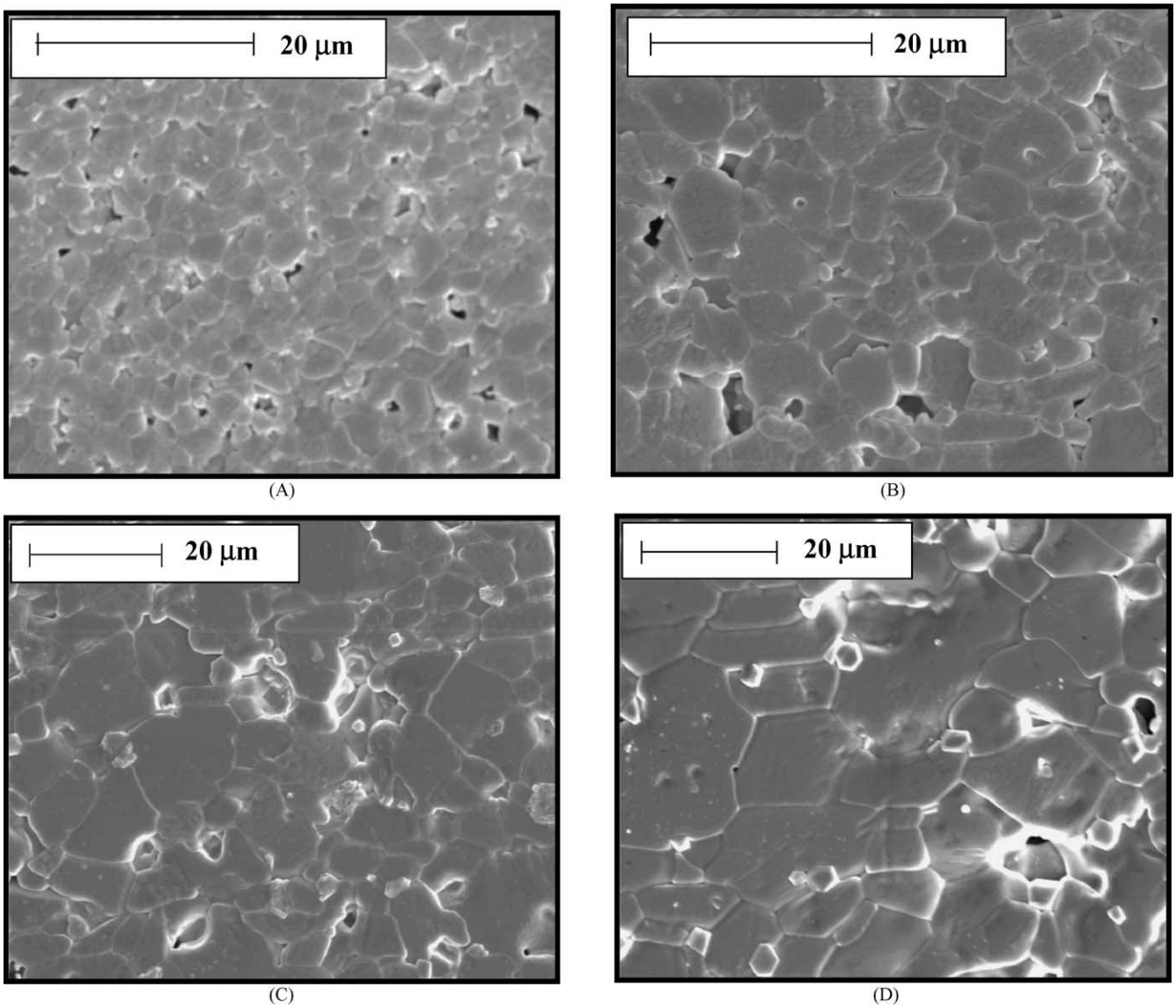

Fig. 12. SEM micrographs of 15T-c samples after sintering at (A) 900 °C, (B) 1000 °C, (C) 1100 °C and (D) 1200 °C for 2 h.

1040 °C individual grains start to grow with the process of exaggerated grain growth.[43]

3.5. Proposed template growth mechanism

Based on the experimental results and discussions, the texture development in ZnO-based varistor systems by the TGG approach can be described schematically as shown in Fig. 11. Initially, anisotropic ZnO templates are oriented parallel to the tape casting direction during the forming process (Fig. 11A). Then, upon heat treatment, prismatic planes of the templates grow faster than other planes and this growth preferentially occurs perpendicular to the tape casting direction (Fig. 11B). In the literature, this anisotropic growth of ZnO prismatic planes has been explained by three different mechanisms:[43,44,46] First, when the atomic arrangement in hexagonal ZnO crystals is considered, the (0 0 0 1) basal planes have atomic populations consisting of either all zinc or oxygen atoms as pointed out by Perkins.[47] If there are no defects like screw dislocations perpendicular to the basal planes, the growth of these planes is hindered significantly. Similarly, the $(1\,1\,\bar{2}\,2)$ pyramidal planes contain only Zn or O atoms; however, their packing density is not as high as that of the basal planes. In contrast, the $(1\,1\,\bar{2}\,0)$ and $(1\,0\,\bar{1}\,0)$ prismatic planes have equal number of zinc and oxygen atoms and hence they are expected to be the leading growth facets on ZnO crystals. That is, the prismatic planes are more preferential to grow than the other ZnO crystal planes due to the atomic arrangements in ZnO crystal structure. Second proposed mechanism is based on the grain growth in the presence of a reactive liquid phase as described earlier. Trontelj et al. qualitatively described that TiO_2 increases the reactivity of the liquid phase toward the ZnO matrix.[42] Therefore, the growth rate difference between the prismatic planes and the other ZnO planes becomes significant and this results in anisotropic grain growth of ZnO crystals. The SEM micrographs, taken from edges of 15T samples (i.e., 15T-c), also support the proposed mechanism and show the faster growth of the prismatic planes, and subsequently, enlargement of the basal planes (Fig. 12). In addition, abnormal grain growth is observed in these microstructures. The faster growth of the prismatic planes of the ZnO templates continue until they impinge each other (Fig. 11C). After impingement, further growth occurs in the *c*-direction (Fig. 11D). The third proposed mechanism for anisotropic grain growth in ZnO-based systems is the effect of the inversion boundaries on the growth of ZnO grains. Makovec et al. reported on exaggerated growth of ZnO grains that contain Ti-rich inversion boundaries. In addition, they found that ZnO grains are elongated in the direction parallel to the inversion boundary line and that Zn_2TiO_4 spinel particles are frequently captured in rapidly growing ZnO grains.[43] Moreover, Daneu and coworkers also reported anisotropic grain growth of ZnO grains doped with small amounts of SnO_2 due to the inversion boundaries.[44] They also discussed possibility of grain size control in ZnO-based ceramics by controlling the number of inversion boundary seed grains (via controlling the initial dopant content). At the present, little is known about the effect of inversion boundaries on the development of textured microstructure in ZnO-based ceramics. However, it is essential to understand how the inversion boundary effect can be utilized in the favor of texture development in TGG-type processes.

4. Conclusions

The present study demonstrates that the TGG approach has been successfully applied to fabricate textured and dense zinc oxide varistors with controlled microstructures. Rod-like, anisotropic ZnO particles (templates) were synthesized by homogeneous precipitation method from 0.01 M zinc nitrate and hexamethylene tetraamine aqueous solutions. The templates are aligned during the modified tape casting process. After the forming, *c*-axes of the templates are oriented in a direction parallel to the tape casting direction. Constrained densification by the template particles has not been observed probably due to the presence of liquid phase during sintering. The aligned zinc oxide templates grow anisotropically during sintering. $(1\,1\,\bar{2}\,0)$ and $(1\,0\,\bar{1}\,0)$ prismatic planes of the ZnO crystals (templates) grow faster than the other ZnO crystal planes. Since orientation can only be controlled in *c*-direction, the growth of the templates results in fiber texture in zinc oxide varistors. As sintering temperature increases, fraction of textured grains in the microstructure increases. These results show that the TGG is a powerful technique to induce texture in zinc oxide-based varistors and it can be applicable other zinc oxide-based ceramics.

Acknowledgements

The authors would like to thank Dr. Aydin Dogan for fruitful discussions throughout this study. In addition, they would like to thank Ms. Nimet Arslan and Mr. M. Uzun for their help during the template synthesis. The financial support from Anadolu University Scientific Research Commission (under the contract number: 020234) for this study is also gratefully acknowledged.

References

1. Matsuoka, M., Nonohmic properties of zinc oxide ceramics. *Jpn. J. Appl. Phys.*, 1971, **10**(6), 736–746.
2. Clarke, D. R., Varistor ceramics. *J. Am. Ceram. Soc.*, 1999, **82**(3), 485–502.
3. Gupta, T. K., Application of zinc oxide varistors. *J. Am. Ceram. Soc.*, 1990, **73**(7), 1817–1840.
4. Eda, K., Inada, M. and Matsuoka, M., Grain growth control in ZnO varistors using seed grains. *J. Appl. Phys.*, 1983, **54**(2), 1095–1099.
5. Hennings, D. F. K., Hartung, R. and Reijnen, P. J., *J. Am. Ceram. Soc.*, 1990, **73**(3), 645–648.
6. Kim, J., Kimura, T. and Yamaguchi, T., Microstructure development in Sb_2O_3-doped ZnO. *J. Mater. Sci.*, 1989, **24**, 2581–2586.

7. Daneu, N., Recnik, A. and Bernik, S., Grain growth control in Sb_2O_3-doped zinc oxide. *J. Am. Ceram. Soc.*, 2003, **86**(8), 1379–1384.
8. Carlson, W. G. and Gupta, T. K., Improved varistor nonlinearity via donor impurity doping. *J. Appl. Phys.*, 1982, **53**, 5746–5753.
9. Miyoshi, T., Maeda, K., Takahashi, K. and Yamazaki, T., Effects of dopants on the characterization of ZnO varistors. In *Advances in Ceramics. Grain Boundary Phenomena in Electronic Ceramics, Vol 1*, ed. L. M. Levinson and D. Hill. American Ceramic Society, Columbus, OH, 1981, p. 309.
10. *Zinc Oxide Rediscovered*. The New Jersey Zinc Company, New York, NY, 1957.
11. Nakamura, Y., Harada, T., Kuribara, H., Kishimoto, A., Motohira and Yanagida, H., Nonlinear, current–voltage characteristics with negative resistance observed at ZnO–ZnO single contacts. *J. Am. Ceram. Soc.*, 1999, **82**(11), 3069–3074.
12. Ellmer, K., Diesner, K., Wendt, R. and Fiechter, S., Relations between texture and electrical parameters of thin polycrystalline zinc oxide films. *Solid State Phenom.*, 1996, **51/52**, 541–546.
13. Chen, J. J., Gao, Y., Zeng, F., Li, D. M. and Pan, F., Effect of sputtering oxygen partial pressures on structure and physical properties of high resistivity ZnO films. *Appl. Surf. Sci.*, 2004, **223**, 318–329.
14. Isobe, S., Tani, T., Masuda, Y., Seo, W. S. and Koumoto, K., Thermoelectric performance of yttrium-substituted $(ZnO)_5In_2O_3$ improved through ceramic texturing. *Jpn. J. Appl. Phys.*, 2002, **41**, 731–732.
15. Suzuki, S. and Sakka, Y., Control of texture in electroceramics by slip-casting in a high magnetic field. *Key Eng. Mater.*, 2003, **248**, 191–194.
16. Messing, G. L., *Textured Ceramics. Encyclopedia of Materials: Science and Technology*. Elsevier Science, Ltd., 2001.
17. Gitzen, W. H., *Alumina as a Ceramic Material*. The American Ceramic Society, Ohio, 1971 (p. 60).
18. Kimura, T., Yashimoto, T., Iida, N., Fujita, Y. and Yamaguchi, T., Mechanisms of grain orientation during hot-pressing of bismuth titanate. *J. Am. Ceram. Soc.*, 1989, **72**, 85–89.
19. Takenaka, T. and Sakata, K., Grain orientation and electrical properties of hot-forged $Bi_4Ti_3O_{12}$ ceramics. *Jpn. J. Appl. Phys.*, 1980, **19**, 31–39.
20. Ma, Y. and Bowman, K. J., Texture in hot-pressed or forged alumina. *J. Am. Ceram. Soc.*, 1991, **74**(11), 2941–2944.
21. Watanabe, H., Kimura, T. and Yamaguchi, T., Sintering of platelike bismuth titanate powder compacts with preferred orientation. *J. Am. Ceram. Soc.*, 1991, **74**(1), 139–147.
22. Seabaugh, M. M., Kerscht, I. H. and Messing, G. L., Texture development by Templated Grain Growth in liquid phase sintered α-alumina. *J. Am. Ceram. Soc.*, 1997, **80**(5), 1181–1188.
23. Seabaugh, M. M., Hong, S. H. and Messing, G. L., Processing of textured ceramics by Templated Grain Growth. In *Ceramic Microstructure: Control at the Atomic Level*, ed. E. P. Tomsia and A. Glaeser. Plenum, New York, 1998, pp. 303–310.
24. Messing, G. L., Seabaugh, M. M. and Hong, S. H., Tailoring microstructure development via Templated Grain Growth. In *Ceramic Processing Science*, ed. G. L. Messing, F. F. Lange and S. Hirano. American Ceramic Society, Westerville, OH, 1998, pp. 497–502.
25. Suvaci, E. and Messing, G. L., Critical factors in the Templated Grain Growth of textured reaction-bonded alumina. *J. Am. Ceram. Soc.*, 2000, **83**(8), 2041–2048.
26. Hirao, K., Nagaoka, T., Brito, M. E. and Kanzaki, S., Microstructure control of silicon nitride by seeding with rod-like β-Si_3N_4 particles. *J. Am. Ceram. Soc.*, 1994, **77**(7), 1857–1862.
27. Hirao, K., Ohashi, M., Brito, M. E. and Kanzaki, S., Processing strategy for producing high anisotropic silicon nitride. *J. Am. Ceram. Soc.*, 1995, **78**(6), 1687–1690.
28. Hirao, K., Watari, K., Brito, M. E., Toriyama, M. and Kanzaki, S., High thermal conductivity in silicon nitride with anisotropic microstructure. *J. Am. Ceram. Soc.*, 1996, **79**(9), 2485–2488.
29. Sacks, M. D., Scheiffele, G. W. and Staab, G. A., Fabrication of textured silicon carbide via seeded anisotropic grain growth. *J. Am. Ceram. Soc.*, 1996, **79**(6), 1611–1616.
30. Sabolsky, E. M., James, A. R., Kwon, S., Trolier-McKinstry, S. and Messing, G. L., Piezoelectric Properties of ⟨0 0 1⟩ textured $Pb(Mg_{1/3}Nb_{2/3})O_3$–$PbTiO_3$ ceramics. *Appl. Phys. Lett.*, 2001, **78**(17), 2551–2553.
31. Brahmaroutu, B., Messing, G. L., Trolier-McKinstry, S. and Selvaraj, U., Templated Grain Growth of textured $Sr_2Nb_2O_7$. In *ISAF'96 Proceedings of the Tenth IEE International Symposium on Applications of Ferroelectrics, Vol II*, ed. B. M. Kulwicki, A. Amin and A. Safari. IEE, Piscataway, NJ, 1996.
32. Horn, J. A., Zhang, S. C., Selvaraj, U., Messing, G. L. and Trolier-McKinstry, S., Templated Grain Growth of textured bismuth titanate. *J. Am. Ceram. Soc.*, 1999, **82**(4), 921–926.
33. Duran, C., Trolier-McKinstry, S. and Messing, G. L., Fabrication and electrical properties of textured Sr0.53Ba0.47Nb2O6 ceramics by Templated Grain Growth. *J. Am. Ceram. Soc.*, 2000, **83**(9), 2203–2213.
34. Hong, S. H. and Messing, G. L., Development of textured mullite by Templated Grain Growth. *J. Am. Ceram. Soc.*, 1999, **82**(4), 867–872.
35. Sakka, Y., Halada, K. and Ozawa, E., Synthesis of ZnO particles by the homogeneous precipitation method. In *Ceramic Transactions—Ceramic Powder Science II, Vol 1*. The American Ceramic Society Inc., 1988.
36. Lotgering, F. K., Topotactical reactions with ferrimagnetic oxides having hexagonal crystal structures—I. *J. Inorg. Nucl. Chem.*, 1959, **9**(2), 113–123.
37. Park, D.-S. and Kim, C.-W., A modification of tape casting for aligning the whiskers. *J. Mater. Sci.*, 1999, **34**, 5827–5832.
38. Suvaci, E., Seabaugh, M. M. and Messing, G. L., Reaction-based processing of textured alumina by Templated Grain Growth. *J. Eur. Ceram. Soc.*, 1999, **19**, 2465–2474.
39. Simpson, Y. K. and Carter, C. B., Faceting behavior of alumina in the presence of a glass. *J. Am. Ceram. Soc.*, 1990, **73**(8), 2391–2398.
40. Burke, J. E., Role of grain boundaries in sintering. *J. Am. Ceram. Soc.*, 1957, **40**(3), 80–85.
41. Harmer, M. P., Bennison, S. J. and Narayan, C., In *Advances in Materials Characterization*, ed. D. R. Rossington, R. A. Condrate and R. L. Snyder. Plenum Press, New York, 1983.
42. Trontelj, M., Kolar, D. and Karsevec, V., Influence of additives on varistor microstructure. In *Advances in Ceramics, Vol 7, Additives and Interfaces in Electronic Ceramics*, ed. M. F. Yan and A. H. Heuer. American Ceramic Society, Columbus, OH, 1983, pp. 107–116.
43. Makovec, D., Kolar, D. and Trontelj, M., Sintering and microstructure development of metal oxide varistor ceramics. *Mater. Res. Bull.*, 1993, **28**(8), 803–811.
44. Daneu, N., Recnik, A., Bernik, S. and Kolar, D., Microstructural development in SnO_2-doped ZnO–Bi_2O_3 ceramics. *J. Am. Ceram. Soc.*, 2000, **83**(12), 3165–3171.
45. Makovec, D. and Trontelj, M., Formation reactions of low-voltage varistor ceramics. *Mater. Sci. Monogr.*, 1991, **66-c**, 2137–2147.
46. Sung, G. Y. and Kim, C. H., Anisotropic grain growth of ZnO grain in the varistor system ZnO–Bi_2O_3–MnO–TiO_2. *Adv. Ceram. Mater.*, 1988, **3**(6), 604–606.
47. Perkins, J., Morphology of ZnO microcrystals. *J. Cryst. Growth*, 1977, **40**, 152–156.